Research Article Vol. 31, No. 10 / 8 May 2023 / Optics Express 16909
Optics EXPRESS

Small lidar ratio of dust aerosol observed by Raman-polarization lidar near desert sources

ZHONGWEI HUANG,[1,2] MEISHI LI,[1] JIANRONG BI,[1,2,*] XINGTAI SHEN,[1] SHUANG ZHANG,[1] AND QIANTAO LIU[1]

[1]Key Laboratory for Semi-Arid Climate Change of the Ministry of Education, College of Atmospheric Sciences, Lanzhou University, Lanzhou 730000, China
[2]Collaborative Innovation Center for West Ecological Safety (CIWES), Lanzhou University, Lanzhou 730000, China
*bijr@lzu.edu.cn

Abstract: Previous studies have shown that the lidar ratio has a significant influence on the retrieval of the aerosol extinction coefficient via the Fernald method, leading to a large uncertainty in the evaluation of dust radiative forcing. Here, we found that the lidar ratios of dust aerosol were only 18.16 ± 14.23sr, based on Raman-polarization lidar measurements in Dunhuang (94.6°E, 40.1°N) in April of 2022. These ratios are much smaller than other reported results (~50 sr) for Asian dust. This finding is also confirmed by some previous results from lidar measurements under different conditions for dust aerosols. The particle depolarization ratio (PDR) at 532 nm and color ratio (CR, 1064 nm/532 nm) of dust aerosols are0.28 ± 0.013 and 0.5-0.6, respectively, indicating that extremely fine nonspherical particles exist. In addition, the dust extinction coefficients at 532 nm range from2×10^{-4} to $6 \times 10^{-4} m^{-1}$for such small lidar ratio particles. Combining lidar measurements and model simulation by the T-matrix method, we further reveal that the reason for this phenomenon is mainly due to the relatively small effective radius and weak light absorption of dust particles. Our study provides a new insight into the wide variation in the lidar ratio for dust aerosols, which helps to better explain the impacts of dust aerosols on the climate and environment.

1. Introduction

Dust aerosols have important impacts on regional and even global ecological environments and climate change [1]. Globally, dust now accounts for a third of all naturally occurring aerosols, equivalent to approximately 600 Mt per year [2]. They not only seriously endanger human health [3] but also affect the properties of clouds and precipitation. Global desertification has a profound and extensive impact on the human living environment [4]. An analysis of 10 sandstorm cases based on satellite data in North China found that dust aerosols inhibited precipitation [5]. The decrease in precipitation caused by dust aerosols caused the soil to become drier, thus producing more dust and providing positive feedback to accelerate the drought process [6]. Moreover, heating of the elevated dust aerosol layer increases the occurrence of deep convection, which in turn strengthens the circulation of the summer monsoon and lead to increased local precipitation [7].

Asian dust has a significant impact on the atmospheric radiation budget balance [8]. Toshiyuki et al. observed that Asian dust generated by sandstorms in high-altitude arid regions of China and Mongolia is easily carried into the troposphere by westerly winds in the spring [9]. To better study the radiation properties of dust aerosols, many field observations have been carried out in arid and semiarid areas of China in recent years [10–17]. Previous studies have shown that one of the important reasons for the uncertainty in the evaluation of the radiation effect of dust aerosols is the lack of observations of their vertical structure [18,19]. Therefore, it is important

#484501 https://doi.org/10.1364/OE.484501
Journal © 2023 Received 28 Dec 2022; revised 23 Feb 2023; accepted 5 Apr 2023; published 5 May 2023

Optics EXPRESS

to study the optical properties and spatial distribution of dust aerosols to estimate the radiation effects of dust aerosols.

Lidar is a very useful tool in atmospheric research since it provides information on several atmospheric parameters with high spatial and temporal resolutions [20]. The measurements of a Mie scattering lidar are generally used to calculate aerosol backscattering and extinction profiles with a fixed lidar ratio assumption in the algorithms [21], which is not conducive to the accurate inversion of aerosol optical properties. In general, when using Mie scattering lidar to retrieve the extinction coefficient of dust aerosol, the lidar ratio is assumed to be approximately 50 sr. The lidar ratio of Asian dust varies between 42 sr and 66 sr in most cases, with a mean of 51 sr [22]. However, it has been noted that the lidar ratio has a great influence on the inversion of the extinction coefficient of aerosols. The factor of 10 range of possible lidar ratios translates into a factor of 10-40 uncertainty in retrieved optical depth. This range is too large to offer an adequate constraint on lidar retrievals for the problems of climate forcing or visibility [23]. Noh et al. observed the presence of pollutants with a lidar ratio of 110 sr at an altitude of more than 1000 meters over East Asia [24]. The lidar ratio of dust aerosol in Lampedusa ranges from 10 to 90 sr, with an average of 30 sr [25]. The lidar ratio varies greatly over time, as observed by sun-photometer and Mie scattering lidar [26]. The lidar ratio and depolarization ratio of dust aerosols from the Taklimakan Desert were higher than those typical for Asian dust in the Kashgar area, located near the edge of the Taklimakan Desert [27]. Some studies have shown that lidar ratio variation is dependent on the regional characteristics of aerosols and atmospheric conditions [28,29]. This means that Mie scattering lidar has limited utility for accurately estimating the optical properties of aerosols. Raman lidar and high spectral resolution lidar (HSRL) can simultaneously and independently measure the extinction coefficient and backscattering coefficient of aerosol [30] without the assumption of parameters, which makes Raman lidar a useful tool for aerosol research. The lidar ratio obtained from Raman lidar observations has very important reference significance for Mie scattering lidar inversion of the extinction coefficient.

To investigate the lidar ratio of dust aerosols near dust sources, we observed the dust vertical structure by using measurements from a ground-based lidar network in Northwest China. The lidar system is a Raman-polarization lidar developed by Lanzhou University, aiming to continuously observe the spatial-temporal distribution of dust aerosols along their long-range transport path. The structure of this paper is organized as follows: the lidar system and methods are presented in detail in Section 2; in Sections 3 and 4, the results and discussion are given; and the conclusions are finally summarized in Section 5.

2. Lidar system and methods

The Raman-polarization lidar used in this study is designed for continuously observing dust aerosols and clouds in the Belt and Road ground-based lidar network (BR-lidarnet) led by Lanzhou University of China [14]. A schematic diagram of the developed Raman-polarization lidar used in this paper is shown in Fig. 1. It employs a Nd:YAG laser emitting a fundamental laser at 1064 nm and converts the 1064 nm laser to a 532 nm laser using a second harmonic generator (SHG). Consequently, a Schmidt Cassegrainian telescope with a diameter of 200 mm is used to receive backscattering signals from the atmosphere. Polarization measurements are achieved at 532 nm to better distinguish dust aerosols from other atmospheric aerosols. The field of view (FOV) of the lidar system is 1 mrad, which can effectively suppress solar radiation during the daytime. Photon counting mode was used at a wavelength of 607 nm, and analog mode was employed at wavelengths of 532 and 1064 nm. The spatial and temporal resolutions are 3.75 m and 5 min, respectively. Raw signals were preprocessed by background subtraction, range correction, polarization calibration and overlap correction [31,32].

Optics EXPRESS

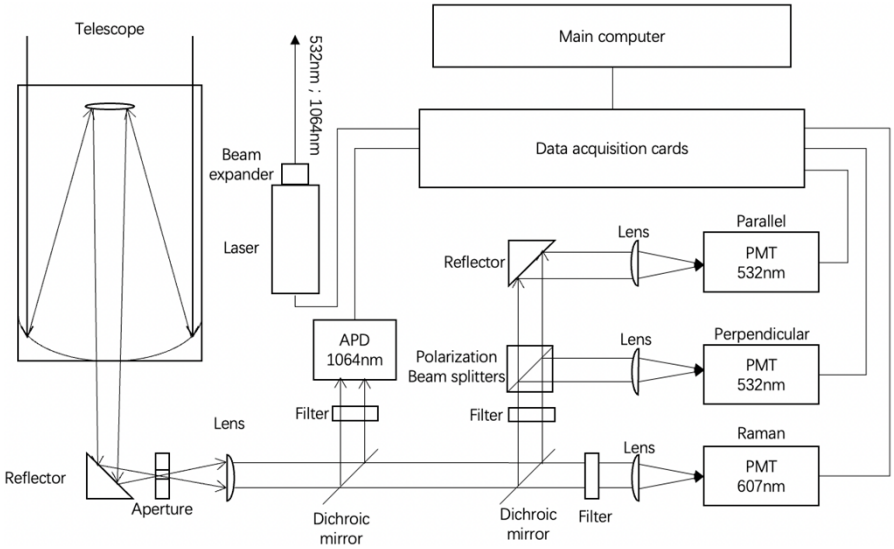

Fig. 1. Schematic diagram of a Raman-polarization lidar designed for lidar network observation in this study.

The aerosol extinction coefficients were given by Eq. (1) [33]:

$$\alpha_{\lambda_0}^{aer}(z) = \frac{\frac{d}{dz} ln\left[\frac{N_{Ref}(z)}{P_{\lambda_{Ref}}(z)z^2}\right] - \alpha_{\lambda_0}^{mol}(z) - \alpha_{\lambda_{Ref}}^{mol}(z)}{1 + \left(\frac{\lambda_0}{\lambda_{Ref}}\right)^k} \tag{1}$$

$N_{Ref}(z)$ is the molecular number density of the Raman scattering at distance z, which is determined by using the standard atmospheric model, and k is the Angstrom exponent, which is usually equal to 1 but depends on aerosol types [33]. α is the extinction coefficient. The superscripts *aer* and *mol* represent aerosol and molecular, respectively. The subscripts λ_0(532 nm) and λ_{Ref}(607 nm) represent the elastic backscattering wavelength and Raman scattering wavelength, respectively. P is the backscattering signal at the Raman channel.

The equation for retrieving aerosol backscatter coefficients by Raman lidar is as follows:

$$\begin{aligned}\beta_{\lambda_0}^{aer}(z) + \beta_{\lambda_0}^{mol}(z) = [\beta_{\lambda_0}^{aer}(z_0) + \beta_{\lambda_0}^{mol}(z_0)] \times \frac{P_{\lambda_{Ref}}(z_0)P_{\lambda_0}(z)N_{Ref}(z)}{P_{\lambda_{Ref}}(z)P_{\lambda_0}(z_0)N_{Ref}(z_0)} \\ \times \frac{exp\left\{-\int_{z_0}^{z}[\alpha_{\lambda_{Ref}}^{aer}(\xi)+\alpha_{\lambda_{Ref}}^{aer}(\xi)]d\xi\right\}}{exp\left\{-\int_{z_0}^{z}[\alpha_{\lambda_0}^{aer}(\xi)+\alpha_{\lambda_0}^{aer}(\xi)]d\xi\right\}}\end{aligned} \tag{2}$$

The reference height z_0 is chosen such that , so that $\beta_{\lambda_0}^{mol}(z_0) + \beta_{\lambda_0}^{aer}(z_0) \approx \beta_{\lambda_0}^{mol}(z_0)$
Finally, the lidar ratio profile can be obtained from the profiles of $\alpha_{\lambda_0}^{aer}(z)$ and $\beta_{\lambda_0}^{aer}(z)$.

$$S_{\lambda_0}^{aer}(z) = \frac{\alpha_{\lambda_0}^{aer}(z)}{\beta_{\lambda_0}^{aer}(z)} \tag{3}$$

The lidar ratio of aerosols is related not only to their shape but also to the wavelength of incident light, spatial orientation, size distribution, complex refractive index and other factors [34,14]. We assume that the aerosol particles are uniform and randomly oriented, and the size distribution is lognormal. Only the effects of the particle effective radius, complex refractive

Optics EXPRESS

index and aspect ratio are considered. For a single particle, the lidar ratio can be calculated by the following formula [35]:

$$S(\lambda) = \frac{4\pi C_{ext}(\lambda)}{a_1(\pi, \lambda) C_{sca}(\lambda)} \tag{4}$$

where C_{ext} and C_{sca} represent extinction cross sections and scattering cross sections of aerosol particles, respectively.

3. Results

The developed Raman-polarization lidar in Dunhuang observed a dust event on April 15, 2022, and continued to observe this dust event, as shown in Fig. 2. From the observation results of lidar, it can be seen that the dust event occurred at approximately 11:00 am Beijing time and lasted for approximately 24 hours. Through the observation results of lidar, it can be found that there was an interesting phenomenon in the dust event in Dunhuang, the source area of the dust. Approximately 12 hours after the dust event, the dust layer gradually rose to approximately 2000 meters above the ground. Similar phenomena have also been observed in Europe with consistency until the end of the dust event [36]. One study found that dust in the Taklimakan Desert can rise up to 4 km above the ground [37]. To analyze the change in the microphysical properties of the dust aerosol in the transmission process of the dust event, lidar observations were also carried out in Zhangye, which falls on the dust transmission path. The observation results of the lidar showed that after approximately 15 hours, the dust particles were transmitted from Dunhuang to Zhangye, and the intensity of the dust observed in Zhangye was relatively weak. This situation indicates that there is an obvious settlement process of dust particles in the transmission process, which can also be illustrated by the observation that the dust particles in Zhangye stretch from the ground to 3,000 meters in the air. The depolarization ratio of dust particles observed in Zhangye is obviously smaller than that in Dunhuang, indicating that the dust particles settling are mainly particles with poor sphericity.

To avoid damage to the PMT caused by noise from sunlight, the Raman channel only works at night. Due to the low signal-to-noise ratio of the Raman channel, the average of the Raman channel was conducted for 2 hours; the time selected is the red dotted line. When the Raman channel is used to determine β^{aer}, at an altitude of 5.6 km, assuming $\beta^{aer} = 0$ and below 200 m, the signal is considered to be coming from the lidar blind spot. When using the least squares method to estimate the slope of the Raman signal, the vertical resolution of the lidar is reduced to 187.5 m. The vertical structure of dust in Dunhuang and Zhangye is shown in (a) and (b) of Fig. 3.

The vertical profile of aerosol optical properties is shown in Fig. 3. As shown in Fig. 3(a), the extinction coefficient and lidar ratio are large below 1000 m, indicating that there is a layer of highly concentrated and highly extinct particles at this height; the lidar ratio above 1000 m is approximately 20 sr, and the vertical structure changes are not obvious. This situation indicates that the dust particles at this height are relatively simple in nature. The extinction coefficient results indicate the presence of an aerosol layer in the vicinity of 2000 m to 2,750 m, proving that the dust layer was raised to more than 2000 m above ground level. Dong et al. also observed dust from the Taklimakan Desert at an altitude of 2-4 km [37]. The PDR result is approximately 0.3 for the strongest dust extinction near 2750 m, which is typical for Asian dust, indicating that the main composition of this layer is indeed dust particles. The PDR results decrease rapidly above 2750 m, indicating that the top of the dust layer was within 3000 m. The variation in PDR results below 2750 m is relatively small, indicating that the dust properties were relatively simple within the whole height. In Fig. 3(b), there is also a layer of particles with high concentration and strong extinction similar to Dunhuang below 1000 m, we speculate that it may be caused by the error of urban aerosol and overlap. Above 1000 m, the extinction coefficient is approximately $2 \times 10^{-4} m^{-1}$, which is lower than that of Dunhuang, indicating that the dust particles were settling

Optics EXPRESS

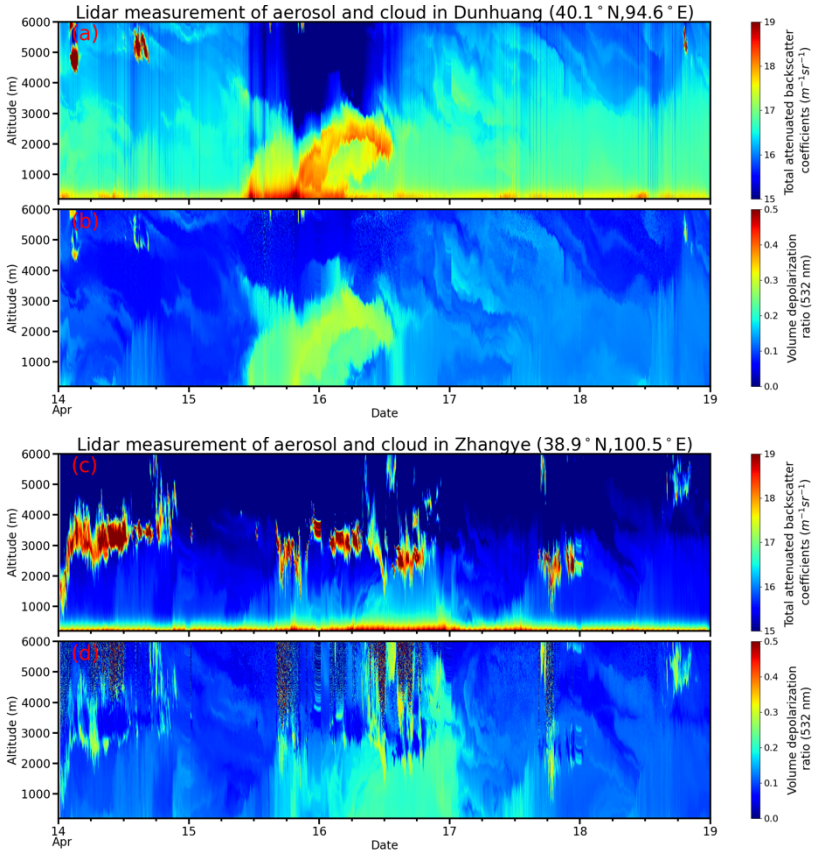

Fig. 2. Vertical structure of aerosols and clouds observed by Raman-polarization lidar in Dunhuang and Zhangye in April 2022.

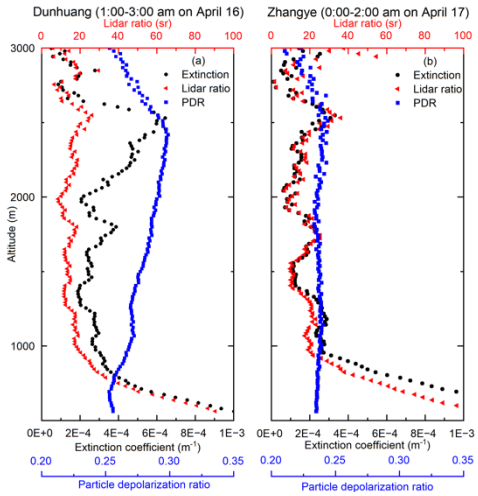

Fig. 3. Vertical profiles of the extinction coefficient, lidar ratio and particle depolarization ratio (PDR) in Dunhuang (a) during 1:00-3:00 am on April 16 and Zhangye (b) during 0:00-2:00 am on April 17.

Optics EXPRESS

during the transport process. The lidar ratio is approximately 20 sr, the PDR changes little, and the PDR value is approximately 0.23, indicating that the settling particles were particles with poor sphericity. Several studies have shown that the nonsphericity of the dust particles determines a significant reduction in the backscattering efficiency, ultimately resulting in an increase in the liar ratio compared to the same size distribution of the star particles [38,39]. Our observation results show that there is no significant difference in the lidar ratio between Dunhuang and Zhangye, which may be caused by the nonsphericity of dust particles and other factors.

We performed a more detailed statistical analysis of the lidar data than the data collected from all data points at altitudes of 600-3000 m, as dust aerosols are not always present at higher altitudes (Fig. 4). During the entire dust event, 60 lidar ratio profiles were acquired. The reason for the low number of profiles is the low signal-to-noise ratio of the Raman signal, which does not always allow successful retrieval of aerosol optical properties when using the Raman method. However, a review of more than 7,000 data points is sufficient for detailed statistical analysis. The lidar ratio ranges from 5.2 to 101.6 sr. This distribution is wider than the previously reported lidar ratio of Asian dust, which is thought to be caused by errors in overlap and mixing of urban aerosols and dust aerosols near the ground. Approximately 58% of the lidar ratio is in the range of 10-15 sr, indicating that the dust generated in Dunhuang was very uniform. This number can be used to represent the lidar ratio of the dust generated at Dunhuang. Approximately 81% of the lidar ratios are in the range of 0-20, which is consistent with the results that most of the lidar ratios of dust from Northwest China observed in Nanjing are less than 20 sr [33].

4. Discussion

Many scholars have observed that the lidar ratio of dust is less than the typical value. Zhang et al. observed some high dust in the middle of the Taklimakan Desert with a lidar ratio of less than 20 sr using Raman lidar [40]. Dust from northwest China, with a lidar ratio of approximately 10 sr, was observed by Raman lidar in Nanjing [33]. A lidar ratio of approximately 22 sr of Saharan dust invading the Mediterranean was reported at Potentsa [42]. Guerrero-Rascado et al. observed a 20-25 sr Saharan dust lidar ratio [20]. Zhu et al. observed the lidar ratio of dust aerosols of 16-30 sr using HSRL [42]. Ackermann modeled lidar ratio values for different tropospheric aerosol types using climatological values of aerosol size distribution to obtain values ranging from 22-25 sr, 20-25 sr and 60-65 sr at 532 nm for maritime, dust and continental aerosols, respectively [43]. We organized some of these results and show them in Fig. 5 [20,25,26,33,40–42,44–55]. It can be clearly seen from Fig. 5 that these scholars all observed the existence of lidar ratios less than 40 sr or even less than 30 sr. Therefore, we can assume that such a small lidar ratio is not an uncommon situation.

To explore the factors affecting the lidar ratio of dust particles, the PDR, color ratio (CR) and extinction coefficient of particles during the whole dust event were counted; the results are shown in Fig. 6. Data with a frequency lower than 0.1% in statistics are considered incidental errors generated in the inversion process and are discarded. According to the results, CR is mainly concentrated in the range of 0.5-0.6 and mainly concentrated at approximately 0.55. Therefore, we can assume that the CR of the dust generated in Dunhuang is approximately 0.55, which is relatively small for dust particles [56,57]. Therefore, we can assume that the small effective radius of the particles is an important reason for the small lidar ratio observed. The extinction coefficient is concentrated at $2 \times 10^{-4} - 6 \times 10^{-4} m^{-1}$, which is higher than the result observed by Zhang et al [40]. in the Taklimakan Desert. It can be seen from the figure that when the extinction coefficient is $2 \times 10^{-4} m^{-1}$, the lidar ratio tends to increase obviously, suggesting that a higher dust concentration leads to a lower lidar ratio. Figure 6(c) shows that PDR is not a factor affecting the lidar ratio at Dunhuang, and the previously reported nonsphericity of particles leading to an increase in the lidar ratio has not been observed [38,39]. When the CR of the dust

Optics EXPRESS

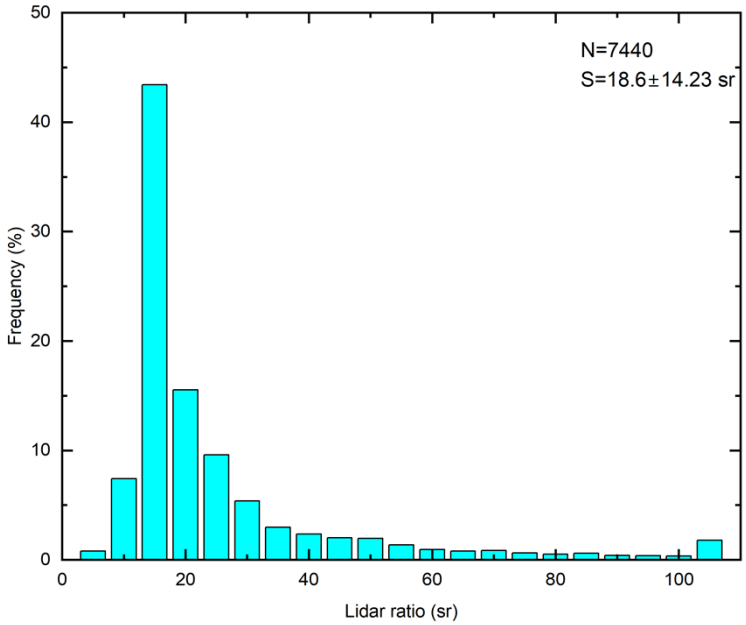

Fig. 4. Possibility distribution of the dust lidar ratio at 532 nm retrieved from Raman-polarization lidar measurements in Dunhuang during 14-17 April 2022.

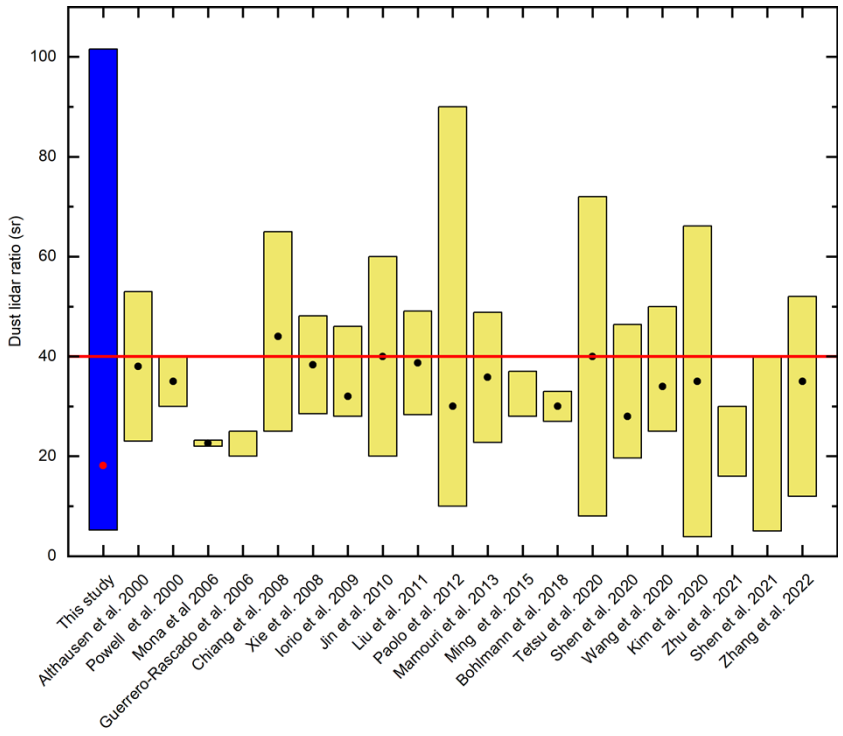

Fig. 5. Comparison of lidar ratios of dust aerosols in this study and those reported in the literature. Black points represent averaged values.

Optics EXPRESS

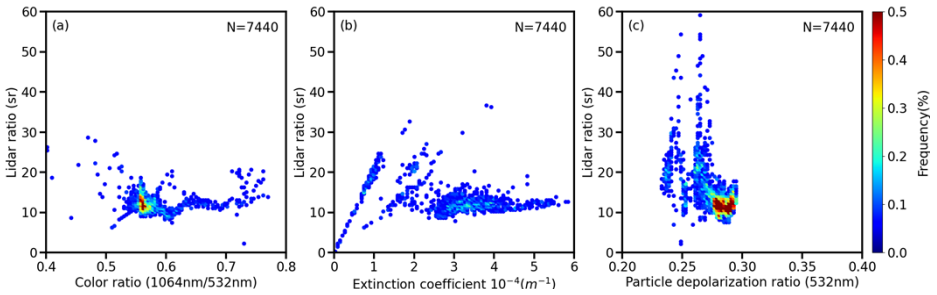

Fig. 6. Relationship between lidar ratio and CR (1064 nm/532 nm), extinction coefficient and PDR (532 nm) of aerosols retrieved from Raman-polarization lidar measurements in Dunhuang during April 14-17, 2022.

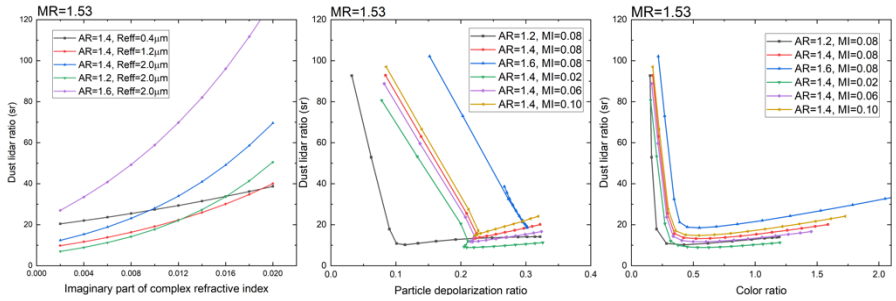

Fig. 7. Effects of aerosol microphysical properties on lidar ratio for dust aerosol simulated using the T-matrix method. The real part of the complex refractive index is assumed to be 1.53 for dust aerosols during the simulation in this study.

particles is between 0.5-0.6 and the extinction coefficient is between $2 \times 10^{-4} - 6 \times 10^{-4} m^{-1}$, we can assume that the lidar ratio of the dust particles is 15 sr.

The T-matrix method can simulate the optical properties and lidar ratio of dust particles with high precision [58]. In this study, the aerosol distribution is assumed to be lognormal. The color ratio (CR), particle depolarization ratio (PDR) and imaginary part of the complex refractive index (MI) are considered. The simulation results are shown in Fig. 7. MR represents the real part of the complex refractive index. Figure 7(a) showed that the lidar ratio of the particle was positively correlated with the imaginary part of the complex refractive index of the particle, and MI may cause very large changes in the lidar ratio of the particle. Therefore, the small lidar ratio observed in Dunhuang may be related to the weak absorption of local dust particles. Dunhuang is a dust source area, and the generated dust aerosol has not mixed with other aerosol particles, so the absorption was weak, which is consistent with the simulation results. Figure 7(b) showed the scatterplot relationship of PDR versus the lidar ratio. The lidar ratio is positively correlated with the PDR, which is consistent with the previously reported results that the non-spherical particle can lead to an increase of the lidar ratio [36]. However, the PDR is not sensitive, indicating that the PDR may not be the main factor affecting the lidar ratio. Similarly, the PDR of dust aerosols observed in Zhangye is smaller than that in Dunhuang, and there is no significant difference for the lidar ratio. This verified that the PDR may not be the reason for the small lidar ratio observed. Figure 7(c) showed the influence of the color ratio on the lidar ratio. When the color ratio was less than 0.4, the lidar ratio was significantly negative correlation with the color ratio, and the change was very drastic. When the color ratio of the particle was greater than 0.4, the lidar ratio was positively correlated with the color ratio, but it was not obvious, which may explain the lidar ratio of less than 20 sr observed by Zhang et al. in the Taklimakan Desert [41]. However, after

Optics EXPRESS

the long-distance transmission of particles, most of the large particles settle, so the lidar ratio may be larger in areas far away from the dust source, which may be the reason for some observed large lidar ratios [24].

5. Conclusion

The lidar ratio is very important for retrieving the aerosol extinction coefficient from widely used Mie scattering lidar measurements. To better investigate the dust lidar ratio near dust sources, we developed a Raman-polarization lidar system for continuously observing dust aerosols in Dunhuang (94.6°E, 40.1°N), northwest China. We found that the lidar ratio of dust aerosol generated in Dunhuang was 18.16 ± 14.23sr, which much smaller than the reported results (~50 sr) for Asian dust based on lidar measurements in April 2022. The PDR at 532 nm and CR (1064 nm/532 nm) of dust aerosols were 0.28 ± 0.013 and 0.5-0.7, respectively, indicating that these particles were fine mode and nonspherical. In addition, dust extinction coefficients at 532 nm ranged from2×10^{-4} to $6 \times 10^{-4} m^{-1}$ for the small lidar ratio particles observed during the studied period. Further analysis that combined the results via the T-matrix method showed that the larger the MI and PDR of dust aerosol corresponded to a larger the lidar ratio of dust aerosol. When the CR of dust aerosol was 0.4~0.8, the lidar ratio of dust aerosol was the smallest, indicating that a smaller or larger effective radius leads to a larger lidar ratio. Combining lidar measurements and model simulation by the T-matrix method revealed that the reason for this phenomenon was the relatively small effective radius and weak absorption of dust particles. This study showed that there were many factors affecting the lidar ratio, and it was necessary to select the appropriate lidar ratio according to different particle characteristics. For dust aerosols, the lidar ratio was assumed to be 15 sr, while the CR is between 0.5 and 0.7. Our study provided a new insight into the wide variation in the lidar ratio for dust aerosols, which helps to better explain the impacts of dust aerosols on the climate and environment when using CALIPSO lidar or ground-based Mie lidar observations. In the future, the lidar ratio of dust aerosol would be further investigated using lidar measurements from the first space-borne high spectral resolution lidar (HSRL) launched by China on April 28, 2022.

Funding. Gansu Provincial Science and Technology Innovative Talent Program: High-level Talent and Innovative Team Special Project (No.22JR9KA001); Fundamental Research Funds for the Central Universities (lzujbky-2022-kb10, lzujbky-2022-kb11); 111 Project (B 13045); the Second Tibetan Plateau Scientific Expedition and Research Program (2019QZKK0602).

Acknowledgments. We thank the code community for providing technical assistance and valuable tools for data analysis and visualization. Thanks for the T-matrix code provided by Prof. M. I. Mishchenko (http://www.giss.nasa.gov/staff/mmishchenko/t_matrix.html).

Disclosures. The authors declare no conflicts of interest.

Data availability. Data underlying the results presented in this paper are not publicly available at this time but may be obtained from the authors upon reasonable request.

Reference

1. J. Xiong, T. Zhao, Y. Bai, Y. Liu, Y. Han, and C. Guo, "Climate characteristics of dust aerosol and its transport in major global dust source regions – ScienceDirect," J. Atmos. Sol.-Terr. Phys. **209**, 105415 (2020).
2. S. Chen, J. Liu, X. Wang, S. Zhao, J. Chen, M. Qiang, B. Liu, Q. Xu, D. Xia, and F. Chen, "Holocene dust storm variations over Northern China: transition from a natural forcing to an anthropogenic forcing," Sci. Bull. **66**(24), 2516–2527 (2021).
3. H. Yan, C. Wang, Z. Niu, and Y. Zhang, "Remote sensing study of tranks and source areas of eastern Asian dust," Progress in Geography. **21**(1), 7 (2002).
4. Y. Han, X. Dai, X. Fang, Y. Chen, and F. Kang, "Dust aerosols: A possible accelerant for an increasingly arid climate in North China," Journal of Arid Environments. **72**(8), 1476–1489 (2008).
5. J. Huang, P. Minnis, B. Lin, T. Wang, Y. Yi, Y. Hu, S. Sunmack, and K. Ayers, "Possible influences of Asian dust aerosols on cloud properties and radiative forcing observed from MODIS and CERES," Geophys. Res. Lett. **33**(6), L06824 (2006).
6. D. Rosenfeld, Y. Rudich, and R. Lahav, "Desert dust suppressing precipitation: A possible desertification feedback loop," Proc. Natl. Acad. Sci. U. S. A. **98**(11), 5975–5980 (2001).

Optics EXPRESS

7. GL. Stephens, NB. Wood, and LA. Pakula, "On the radiative effects of dust on tropical convection," Geophys. Res. Lett. 31(23), (2004).
8. M. Uematsu, R. A. Duce, J. M. Prospero, L. Chen, J. T. Merrill, and R. L. McDonald, "Transport of mineral aerosol from Asia Over the North Pacific Ocean," J. Geophys. Res. **88**(C9), 5343–5352 (1983).
9. T. Murayama, N. Sugimoto, and I. Uno, *et al.*, "Ground-based network observation of Asian dust events of April 1998 in east Asia," J. Geophys. Res. **106**(D16), 18345–18359 (2001).
10. D. Tanré, J. Haywood, J. Pelon, J. F. Léon, B. Chatenet, P. Formenti, P. Francis, P. Goloub, E. J. Highwood, and G. Myhre, "Measurement and modeling of the Saharan dust radiative impact: Overview of the Saharan Dust Experiment (SHADE)," J. Geophys. Res. **108**(D18), 8574 (2003).
11. J. L. Stith, V. Ramanathan, W. A. Cooper, G. C. Roberts, P. J. DeMott, G. Carmichael, C. D. Hatch, B. Adhikary, C. H. Twohy, D. C. Rogers, D. Baumgardner, A. J. Prenni, T. Campos, R. Gao, J. Anderson, and Y. Feng, "An overview of aircraft observations from the Pacific Dust Experiment campaign," J. Geophys. Res. **114**(D5), D05207 (2009).
12. Z. Huang, J. Huang, J. Bi, G. Wang, W. Wang, Q. Fu, Z. Li, S. C. Tsay, and J. Shi, "Dust aerosol vertical structure measurements using three MPL lidars during 2008 China-U.S. joint dust field experiment," J. Geophys. Res. **115**(D7), D00K15 (2010).
13. Z. Huang, JB. Nee, CW. Chiang, S. Zhang, H. Jin, W. Wang, and T. Zhou, "Real-time observations of dust–cloud interactions based on polarization and Raman lidar measurements," Remote Sensing **10**(7), 1017 (2018).
14. Z. Huang, S. Qi, T. Zhou, Q. Dong, and J. Shi, "Investigation of aerosol absorption with dual-polarization lidar observations," Opt. Express **28**(5), 7028 (2020).
15. X. Ma, Z. Huang, S. Si, J. Huang, S. Zhang, Q. Dong, and X. Wang, "Ten-year global particulate mass concentration derived from space-borne CALIPSO lidar observations," Sci. Total Environ. **721**, 137699 (2020).
16. S. Qi, Z. Huang, X. Ma, J. Huang, T. Zhou, S. Zhang, Q. Dong, J. Bi, and J. Shi, "Classification of atmospheric aerosols and clouds by use of dual-polarization lidar measurements," Opt. Express **29**(15), 23461–23476 (2021).
17. Z. Huang, J. Huang, T. Hayasaka, S. Wang, T. Zhou, and H. Jin, "Short-cut transport path for Asian dust directly to the Arctic: a case study," Environ. Res. Lett. **10**(11), 114018 (2015).
18. A. Zhu, V. Ramanathan, Fang Li, and D. Kim, "Dust plumes over the Pacific, Indian, and Atlantic oceans: Climatology and radiative impact," J. Geophys. Res. **112**(D16), D16208 (2007).
19. T. Nousiainen, "Optical modeling of mineral dust particles: A review," J. Quant. Spectrosc. Radiat. Transfer **110**(14-16), 1261–1279 (2009).
20. J. L. Guerrero-Rascado, B. Ruiz, and L. Alados-Arboledas, "Multi-spectral Lidar characterization of the vertical structure of Saharan dust aerosol over southern Spain," Atmos. Environ. **42**(11), 2668–2681 (2008).
21. F. G. Fernald, "Analysis of atmospheric LIDAR observations: Some comments," Appl. Opt. **23**(5), 652–653 (1984).
22. Z. Liu, N. Sugimoto, and T. Murayama, "Extinction-to-backscatter ratio of Asian dust observed with high-spectral-resolution lidar and Raman lidar," Appl. Opt. **41**(15), 2760 (2002).
23. S. J. Doherty, T. L. Anderson, and R. J. Charlson, "Measurement of the lidar ratio for atmospheric aerosols with a 180° backscatter nephelometer," Appl. Opt. **38**(9), 1823–1832 (1999).
24. Y. M. Noh, Y. J. Kim, B. C. Choi, and T. Murayama, "Aerosol lidar ratio characteristics measured by a multi-wavelength Raman lidar system at Anmyeon Island, Korea," Atmos. Res. **86**(1), 76–87 (2007).
25. T. Di Iorio, A. di Sarra, D. M. Sferlazzo, M. Cacciani, D. Meloni, F. Monteleone, D. Fuà, and G. Fiocco, "Seasonal evolution of the tropospheric aerosol vertical profile in the central Mediterranean and role of desert dust," J. Geophys. Res. **114**(D2), D02201 (2009).
26. J. Shen and N. Cao, "Comprehensive observation and analysis of aerosol optical properties and vertical distribution in Nanjing, China," Atmos. Environ. **239**(2), 117767 (2020).
27. Q. Hu, H. Wang, P. Goloub, Z. Li, I. Veselovskii, T. Podvin, K. Li, and M. Korenskiy, "The characterization of Taklamakan dust properties using a multiwavelength Raman polarization lidar in Kashi, China," Atmos. Chem. Phys. **20**(22), 13817–13834 (2020).
28. D. Müller, I. Mattis, U. Wandinger, A. Ansmann, D. Althausen, O. Dubovik, S. Eckhardt, and A. Stohl, "Saharan dust over a central European EARLINET-AERONET site: combined observations with Raman lidar and Sun photometer," J. Geophys. Res. **108**(D12), 4345 (2003).
29. T. Murayama, D. Müller, K. Wada, A. Shimizu, M. Sekiguchi, and T. Tsukamoto, "Characterization of Asian dust and Siberian smoke with multi-wavelength Raman lidar over Tokyo, Japan in spring 2003," Geophys. Res. Lett. **31**(23), 103 (2004).
30. A. Ansmann, U. Wandinger, M. Riebesell, C. Weitkamp, and W. Michaeli, "Independent measurement of extinction and backscatter profiles in cirrus clouds by using a combined Raman elastic-backscatter lidar," Appl. Opt. **31**(33), 7113 (1992).
31. W. Wang, W. Gong, F. Mao, and Z. Pan, "Physical constraint method to determine optimal overlap factor of Raman lidar," J. Opt. **47**(1), 83–90 (2018).
32. L. Mei, T. Ma, Z. Zhang, R. Fei, K. Liu, Z. Gong, and H. Li, "Experimental calibration of the overlap factor for the pulsed atmospheric lidar by employing a collocated Scheimpflug lidar," Remote Sensing **12**(7), 1227 (2020).
33. J. Shen, N. Cao, and Y. Zhao, "Accurate retrieval of aerosol lidar ratio by Raman-Mie lidar in Nanjing," Optik (Munich, Ger.) **227**, 165980 (2021).
34. Q. Xu, D. Wang, X. Wang, and Z. Wu, "Computation and analysis on scattering characteristics of single nonspherical particles of atmospheric haze by T matrix algorithm," Infrared and Laser Engineering. **46**(11), 1117003 (2017).

Optics EXPRESS

35. O. Dubovik, A. Sinyuk, T. Lapyonok, B. N. Holben, M. Mishchenko, P. Yang, T. F. Eck, H. Volten, O. Muñoz, B. Veihelmann, W. J. van der Zande, J. F. Leon, M. Sorokin, and I. Slutsker, "Application of spheroid models to account for aerosol particle nonsphericity in remote sensing of desert dust," J. Geophys. Res. **111**(D11), D11208 (2006).
36. D. M. Powell, J. A. Reagan, M. A. Rubio, W. H. Erxleben, and J. D. Spinhirne, "ACE-2 multiple angle micro-pulse lidar observations from Las Galletas, Tenerife, Canary Islands," Tellus. **52**(2), 652–661 (2000).
37. Q. Dong, Z. Huang, W. Li, Z. Li, X. Song, W. Liu, T. Wang, J. Bi, and J. Shi, "Polarization lidar measurements of dust optical properties at the junction of the Taklimakan Desert–Tibetan Plateau," Remote Sens. **14**(3), 558 (2022).
38. M. I. Mishchenko, L. D. Travis, R. A. Kahn, and R. A. West, "Modeling phase functions for dustlike tropospheric aerosols using a mixture of randomly oriented polydisperse spheroids," J. Geophys. Res. **102**(D14), 16831–16847 (1997).
39. Z. Liu, A. Omar, M. Vaughan, J. Hair, C. Kittaka, Y. Hu, K. Powell, C. Trepte, D. Winker, C. Hostetler, R. Ferrare, and R. Pierce, "CALIPSO lidar observations of the optical properties of Saharan dust: A case study of long-range transport," J. Geophys. Res. **113**(D7), D07207 (2008).
40. S. Zhang, Z. Huang, M. Li, X. Shen, Y. Wang, Q. Dong, J. Bi, J. Zhang, W. Li, Z. Li, and X. Song, "Vertical structure of dust aerosols observed by a ground-based Raman lidar with polarization capabilities in the center of the Taklimakan Desert," Remote Sens. **14**(10), 2461 (2022).
41. L. Mona, A. Amodeo, M. Pandolfi, and G. Pappalardo, "Saharan dust intrusions in the Mediterranean area: Three years of Raman lidar measurements," J. Geophys. Res. **111**(D16), D16203 (2006).
42. S. Zhu, L. Bu, and J. Liu, "Study on airborne high spectral resolution lidar detecting optical properties and pollution of atmospheric aerosol," Chin. J. Lasers. **48**(17), 1710003 (2021).
43. J. Ackermann, "The extinction-to-backscatter ratio of tropospheric aerosol: a numerical study," J. Atmos. Oceanic Technol. **15**(4), 1043–1050 (1998).
44. D. Althausen, D. Müller, A. Ansmann, U. Wandinger, H. Hube, E. Clauder, and S. Zörner, "Scanning 6-wavelength 11-channel aerosol lidar," J. Atmos. Oceanic Technol. **17**(11), 1469–1482 (2000).
45. C. W. Chiang, S. K. Das, and J. B. Nee, "An iterative calculation to derive extinction-to-backscatter ratio based on lidar measurements," J. Quant. Spectrosc. Radiat. Transfer **109**(7), 1187–1195 (2008).
46. C. Xie, T. Nishizawa, N. Sugimoto, I. Matsui, and Z. Wang, "Characteristics of aerosol optical properties in pollution and Asian dust episodes over Beijing, China," Appl. Opt. **47**(27), 4945 (2008).
47. Y. Jin, K. Kai, T. Shibata, K. Zhang, and H. Zhou, "Validation of the dust layer structure over the Taklimakan Desert, China by the CALIOP space-borne lidar using ground-based lidar," Sola **6**, 121–124 (2010).
48. J. Liu, Y. Zheng, Z. Li, C. Flynn, E. J. Welton, and M. Cribb, "Transport, vertical structure and radiative properties of dust events in southeast China determined from ground and space sensors," Atmos. Environ. **45**(35), 6469–6480 (2011).
49. P. D. Girolamo, D. Summa, R. Bhawar, T. D. Iorio, M. Cacciani, I. Veselovskii, O. Dubovik, and A. Kolgotin, "Raman lidar observations of a Saharan dust outbreak event: Characterization of the dust optical properties and determination of particle size and microphysical parameters – ScienceDirect," Atmos. Environ. **50**(1), 66–78 (2012).
50. R. E. Mamouri, A. Ansmann, A. Nisantzi, P. Kokkalis, A. Schwarz, and D. Hadjimitsis, "Low Arabian dust extinction-to-backscatter ratio," Geophys. Res. Lett. **40**(17), 4762–4766 (2013).
51. Z. Ming, C. Xie, Z. Zhong, B. Wang, Z. Wang, P. Dai, Z. Shang, M. Tan, D. Liu, and Y. Wang, "Development of high spectral resolution lidar system for measuring aerosol and cloud," Journal of the Optical Society of Korea. **19**(6), 695–699 (2015).
52. S. Bohlmann, H. Baars, M. Radenz, R. Engelmann, and A. Macke, "Ship-borne aerosol profiling with lidar over the Atlantic Ocean: from pure marine conditions to complex dust–smoke mixtures," Atmos. Chem. Phys. **18**(13), 9661–9679 (2018).
53. T. Sakai, T. Shibata, Y. Iwasaka, T. Nagai, M. Nakazato, T. Matsumura, A. Ichiki, Y. S. Kim, K. Tamura, D. Troshkin, and S. Hamdi, "Case study of Raman lidar measurements of Asian dust events in 2000 and 2001 at Nagoya and Tsukuba, Japan," Atmos. Environ. **36**(35), 5479–5489 (2002).
54. S. H. Wang, H. W. Lei, S. K. Pani, H. Y. Huang, N. H. Lin, E. J. Welton, S. C. Chang, and Y. C. Wang, "Determination of lidar ratio for major aerosol types over Western North Pacific based on long-term MPLNET data," Remote Sens. **12**(17), 2769 (2020).
55. M. H. Kim, S. W. Kim, and A. H. Omar, "Dust lidar ratios retrieved from the CALIOP measurements using the MODIS AOD as a constraint," Remote Sensing **12**(2), 251 (2020).
56. S. Burton, R. Ferrare, C. Hostetler, J. Hair, R. Rogers, M. Obland, C. Butler, A. Cook, D. Harper, and K. Froy, "Aerosol classification using airborne High Spectral Resolution Lidar measurements-methodology and examples," Atmos. Meas. Tech. **5**(1), 73–98 (2012).
57. Z. Huang, Q. Dong, B. Chen, T. Wang, J. Bi, T. Zhou, K. Alam, J. Shi, and S. Zhang, "Method for retrieving range-resolved aerosol microphysical properties from polarization lidar measurements," Opt. Express **31**(5), 7599–7616 (2023).
58. Z. Huang, X. Shen, S. Tang, T. Zhou, Q. Dong, S. Zhang, M. Li, and Y. Wang, "Simulated depolarization ratios for dust and smoke at laser wavelengths: implications for lidar application," Opt. Express **31**(6), 10541–0553 (2023).